

Metastable skyrmions with various topologies in an ultrathin magnetic film. II. Characterization with scanning tunneling microscopy simulations

Krisztián Palotás^{1,2,*}, Levente Rózsa³, Eszter Simon¹, László Udvardi^{1,4}, and László Szunyogh^{1,4}

1 Budapest University of Technology and Economics,

Department of Theoretical Physics, Budafoki út 8., H-1111 Budapest, Hungary

*2 Slovak Academy of Sciences, Institute of Physics, Department of Complex Physical Systems,
Center for Computational Materials Science, SK-84511 Bratislava, Slovakia*

*3 Hungarian Academy of Sciences, Wigner Research Center for Physics,
Institute for Solid State Physics and Optics, P.O. Box 49, H-1525 Budapest, Hungary*

4 Budapest University of Technology and Economics,

MTA-BME Condensed Matter Research Group, Budafoki út 8., H-1111 Budapest, Hungary

(Dated: May 5, 2022)

We report on the characterization of metastable skyrmionic spin structures with various topological charges ($Q = -3, -2, -1, 0, +1, +2$) in the $(\text{Pt}_{0.95}\text{Ir}_{0.05})\text{Fe}/\text{Pd}(111)$ ultrathin magnetic film, considered as isotropic environment, by performing spin-polarized scanning tunneling microscopy (SP-STM) calculations. We find that an out-of-plane magnetized tip already results in distinguished STM contrasts for the different skyrmions. Using an in-plane magnetized tip, we demonstrate that $|Q|$ can be determined from the image contrast of a single SP-STM measurement. We highlight that an in-plane tip magnetization rotation provides the sign of Q independently on the sign of the effective spin polarization in the tunnel junction. We also discuss the validity of the above findings for strong shape effects observed in skyrmionic systems in an anisotropic environment.

I. INTRODUCTION

Recent experimental observations of topologically protected magnetic skyrmion structures in a variety of systems ranging from bulk chiral magnets [1, 2] through multiferroic materials [3, 4] to thin films [5–7] require theoretical efforts to understand their formation, stability and other physical properties that can be exploited in technological applications [8–10]. An important issue is the study of finite temperature effects on the skyrmion stability [11–13]. So far, the smallest skyrmions have been observed in ultrathin films at low temperature [14], where their diameter can be as small as a few nanometers [15–18]. Such real-space spin structures can conveniently be imaged by using spin-polarized scanning tunneling microscopy (SP-STM) [19–21]. The controlled manipulation (creation and annihilation) of skyrmions by SP-STM [22, 23] is a key to write and delete information in magnetic media. Another important aspect is the systematic understanding of the SP-STM contrasts of skyrmionic structures with different topologies. Dupé et al. reported SP-STM contrast characteristics for a set of metastable skyrmions [21], where they identified circular contrasts using an out-of-plane magnetized tip and two types of contrasts employing an in-plane magnetized tip: (i) a two-lobes contrast for spin structures with topological charge $|Q| = 1$ and (ii) a four-lobes contrast for a higher-order antiskyrmion with $|Q| = 2$. The discovery of other types of metastable skyrmionic structures in the $(\text{Pt}_{0.95}\text{Ir}_{0.05})\text{Fe}/\text{Pd}(111)$ ultrathin magnetic film [24] enables the generalization of the findings of Dupé

et al. for the SP-STM contrasts of topologically distinct skyrmions.

Our work identifies STM contrast rules by investigating metastable skyrmionic spin structures with various topological charges ($Q = -3, -2, -1, 0, +1, +2$) in the $(\text{Pt}_{0.95}\text{Ir}_{0.05})\text{Fe}/\text{Pd}(111)$ ultrathin magnetic film employing SP-STM simulations. We suggest that these rules enable the topological characterization of skyrmionic spin structures (magnitude and sign of Q) based on experimentally measured SP-STM images using a minimum of two linearly independent in-plane tip magnetization orientations. We propose that our STM contrast rules are general for skyrmionic structures in other ultrathin films providing an isotropic environment, and they are not valid in anisotropic environments of skyrmion formation [23, 25], e.g., in reconstructed or confined film geometries, since distorted skyrmion shapes strongly affect the observed STM contrast.

The paper is organized as follows. The Method section describes the employed SP-STM simulation method and parameters used. After that, SP-STM simulation results are presented and discussed, and conclusions are drawn on the relationship between the STM contrast and the skyrmion topology.

II. METHOD

For the simulation of the SP-STM images of the skyrmionic spin structures, the three-dimensional Wentzel-Kramers-Brillouin (3D-WKB) approximation [26] of electron tunneling has been employed, where the tunneling current at the tip apex position \mathbf{R}_{TIP} and bias voltage V is calculated as the superposition of 1D-WKB contributions from the sample surface atoms (sum over

*Electronic address: palotas@phy.bme.hu

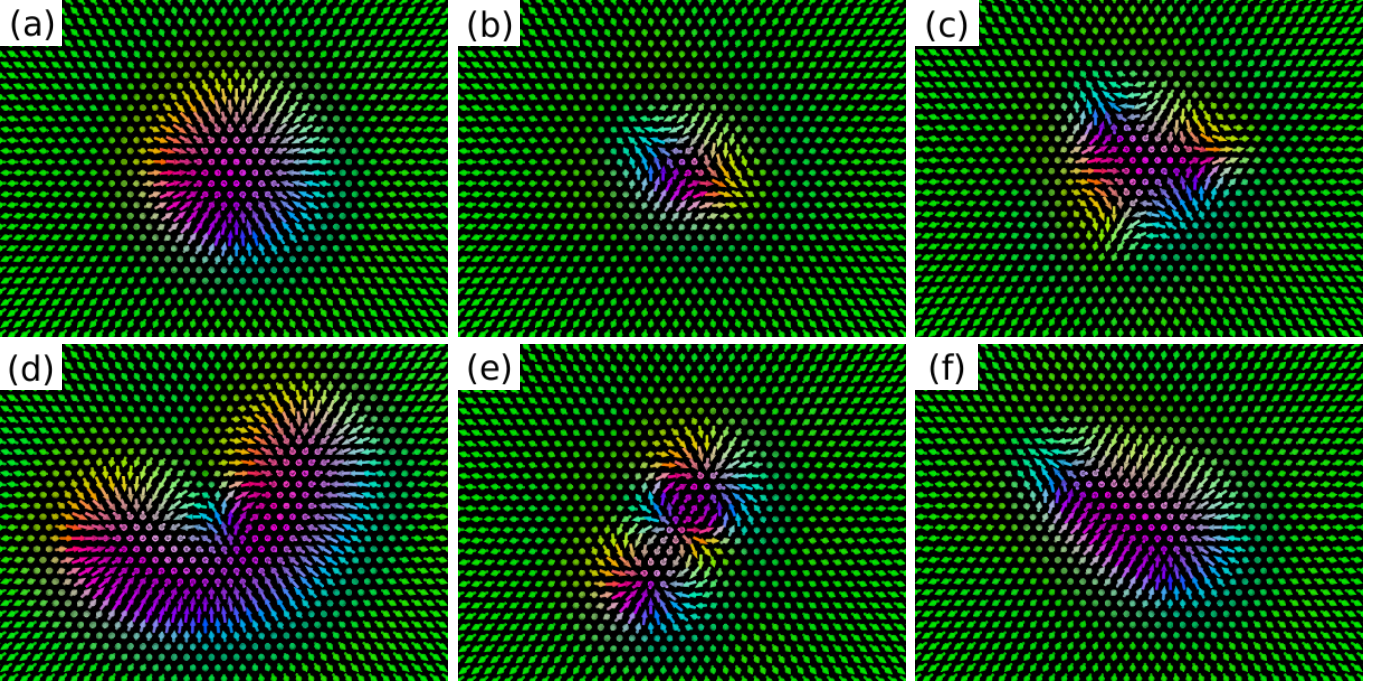


FIG. 1: (Color online) Metastable localized skyrmionic spin configurations with different topological charges in the $(\text{Pt}_{0.95}\text{Ir}_{0.05})\text{Fe}/\text{Pd}(111)$ ultrathin magnetic film: (a) skyrmion with $Q = -1$, (b) antiskyrmion with $Q = 1$, (c) antiskyrmion with $Q = 2$, (d) skyrmion with $Q = -2$, (e) skyrmion with $Q = -3$, (f) “chimera” skyrmion with $Q = 0$. The value of the external field is $B = 0.23$ T (a)-(d),(f) and $B = 2.35$ T (e); the ground state is field-polarized for $B > 0.21$ T.

a) as [27]

$$\begin{aligned}
 I(\mathbf{R}_{TIP}, V) &= \epsilon^2 \frac{e^2}{h} \sum_a \int_0^V dU \\
 &\times \exp \left[-\sqrt{\frac{8m}{\hbar^2} \left(\frac{\Phi_S + \Phi_T + eV}{2} - eU \right)} |\mathbf{R}_{TIP} - \mathbf{R}_a| \right] \\
 &\times n_S^a (E_F^S + eU) n_T (E_F^T + eU - eV) \\
 &\times [1 + P_S^a (E_F^S + eU) P_T (E_F^T + eU - eV) \cos(\phi_a)]. \quad (1)
 \end{aligned}$$

Here, the exponential factor describes the tunneling transmission, where all electron states are assumed as exponentially decaying spherical states [28–30] with an effective rectangular potential barrier in the vacuum between the sample and the tip. The electronic structures enter the model by considering $n_{S(T)}$ the atom-projected charge density of states and $P_{S(T)}$ the spin polarization of the sample surface (S) and the tip apex (T). ϕ_a is the angle of the localized magnetic moment of surface atom a with respect to the tip magnetization direction, e is the elementary charge, \hbar is the (reduced) Planck constant, m is the electron’s mass, and $\Phi_{S(T)}$ and $E_F^{S(T)}$ denote the electron work function and the Fermi energy of the sample surface (tip), respectively. The $\epsilon^2 e^2 / h$ factor ensures the correct dimension of the current. The value of ϵ has to be determined by comparing the simulation results of the charge current with experiments, or with calculations using standard methods, e.g., the Bardeen approach [31]. In our simulations $\epsilon = 1$ eV has been chosen [32] that

gives comparable current values with those obtained by the Bardeen method implemented in the BSKAN code [33, 34]. Note that the choice of ϵ has no qualitative influence on the reported STM contrasts and conclusions.

In the present work, SP-STM images correspond to constant-current contours calculated at the bias voltage $V = 0$ V, where Eq. (1) takes the form [30]:

$$\begin{aligned}
 I(\mathbf{R}_{TIP}) &\propto \sum_a \exp \left[-\sqrt{8m\Phi/\hbar^2} |\mathbf{R}_{TIP} - \mathbf{R}_a| \right] \\
 &\times [1 + P_S P_T \cos(\phi_a)], \quad (2)
 \end{aligned}$$

assuming $P_S^a = P_S$ for all surface atoms and $\Phi = \Phi_S = \Phi_T$. Motivated by a recent work [21], we choose the effective spin polarization of $P_{eff} = P_S P_T = \pm 0.4$ and consider the effect of its sign on the STM contrasts. Electron work functions of $\Phi_S = \Phi_T = 5$ eV were taken. With the selected parameters, the current value $I = 10^{-4}$ nA of the constant-current contours corresponds to about 6 Å minimal tip-sample distance and corrugation values between 30 and 40 pm. Note that smaller corrugation values found in an experiment [20] are either due to a different P_{eff} magnitude or to a larger tip-sample separation in the experiment, for a theoretical explanation of the latter effect see, e.g., Ref. [35]. P_{eff} also plays a crucial role in spin-polarized scanning tunneling spectroscopy [36].

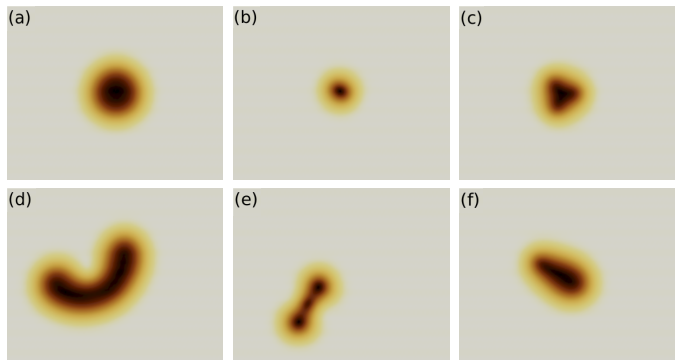


FIG. 2: (Color online) Simulated SP-STM images of the set of skyrmionic spin configurations shown in Fig. 1 using an out-of-plane magnetized tip (pointing in the $+z$ direction) with $P_{eff} = +0.4$. The color scale and image areas are the same for all skyrmionic structures.

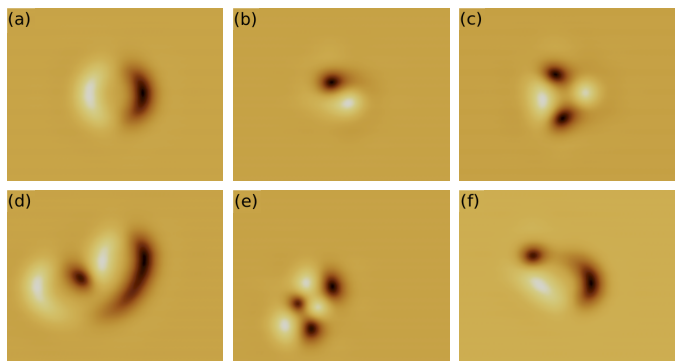


FIG. 3: (Color online) Same as Fig. 2 using an in-plane magnetized tip (pointing in the $+x$ $[1\bar{1}0]$ direction) with $P_{eff} = +0.4$.

III. RESULTS AND DISCUSSION

Figure 1 shows a set of metastable skyrmionic spin structures obtained in a $(\text{Pt}_{0.95}\text{Ir}_{0.05})\text{Fe}/\text{Pd}(111)$ ultrathin magnetic film, where attractive skyrmions have recently been reported [37]. Formation and stability of the metastable structures are extensively discussed in Ref. [24]. Note that the configurations shown in Fig. 1(a)-(c) (first row) have also been reported by Dupé et al. [21]. In the following, we focus on the comparison of our obtained STM contrasts with the work of Dupé et al., and also generalize some of their findings based on our extended set of results on higher-order skyrmions. The characterization of the skyrmionic structures is performed by SP-STM simulations considering different fixed tip magnetization orientations, which are sensitive to the in-line orientation of the local magnetization of the complex surface spin structures, causing the magnetic contrast depending on the sign of P_{eff} . We note that the setting of an arbitrary tip magnetization orientation through a 3D vector field is possible in SP-STM experiments according to Ref. [38].

SP-STM images using an out-of-plane magnetized tip

(pointing in the $+z$ direction) are shown in Figure 2. In case of a positive P_{eff} the ferromagnetic background provides a bright contrast, and the skyrmionic spin structures are imaged as dark regions exhibiting different shapes. The latter finding is in striking difference with Ref. [21]. Strictly speaking, we find a circular contrast for the skyrmion with $Q = -1$ [Fig. 2(a)] only. This circular contrast is distorted for the antiskyrmions: $Q = 1$ shows slightly elongated contrast along a specific axis [Fig. 2(b)], and $Q = 2$ shows a rounded triangular contrast [Fig. 2(c)]. The higher-order skyrmions with $Q = -2$ and $Q = -3$ and the “chimera” skyrmion with $Q = 0$ show non-circular contrasts with an out-of-plane magnetized tip [Fig. 2(d)-(f)]. These observed STM contrasts are in correspondence with the alignment and distortion of the real-space spin structures, and reasons for that are discussed in Ref. [24]. Note that the STM contrasts reported in Fig. 2 are reversed using an out-of-plane magnetized tip pointing in the $-z$ direction keeping the sign of P_{eff} , or keeping the tip magnetization direction in $+z$ and reversing the sign of P_{eff} .

We observe a wider variety of STM contrasts when the tip magnetization is changed from out-of-plane to in-plane. SP-STM images using an in-plane magnetized tip (pointing in the $+x$ $[1\bar{1}0]$ direction) are shown in Figure 3. The two-lobes contrast in Fig. 3(a),(b) has been experimentally observed [20] and the four-lobes contrast in Fig. 3(c) has been calculated [21] earlier. The other spin structures provide more complicated contrast patterns using an in-plane magnetized tip [Fig. 3(d)-(f)]. In general, we find the following trend: the number of bright and dark spots equals for each case shown in Fig. 3(a)-(e) with an alternating order along the perimeter of the skyrmions, and the number of one type of spots (bright or dark) equals the absolute value of the topological charge, $|Q|$. This is understandable since the topological charge can be interpreted as a winding number (vorticity), i.e., how many times are the spins rotated in the plane when passing around the perimeter of the skyrmion once. Given the fixed tip magnetization direction, this selects the number $|Q|$ of bright and dark contrast regions corresponding to parallel and antiparallel alignments of the surface spin structure with respect to the magnetization direction of the tip (for $P_{eff} > 0$). This is in agreement with our expectations in view of the theory of higher-order skyrmions, see, e.g., Ref. [24]. A special case is presented in Fig. 3(f): the “chimera” skyrmion with $Q = 0$. Here, one bright and two dark spots are observed, and this scenario does not correspond to our previous interpretation because the in-plane rotation of the spins along the perimeter is changing direction [see Fig. 1(f)] providing zero Q . We return to this case after studying the effect of the tip magnetization rotation on the in-plane STM contrast. Note that the STM contrasts reported in Fig. 3 are reversed using an in-plane magnetized tip pointing in the $-x$ direction keeping the sign of P_{eff} , or keeping the tip magnetization direction in $+x$ and reversing the sign of P_{eff} .

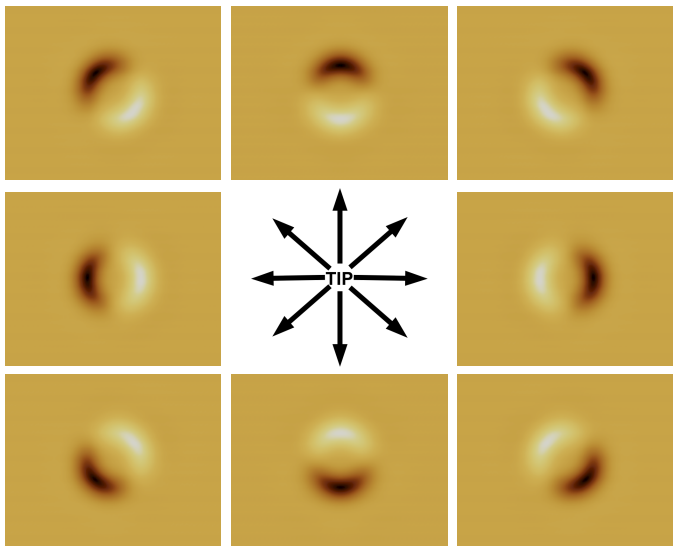


FIG. 4: (Color online) Simulated SP-STM images for the skyrmion with $Q = -1$ by rotating the tip magnetization direction in the surface plane using $P_{eff} = +0.4$. The color scale is the same for all images.

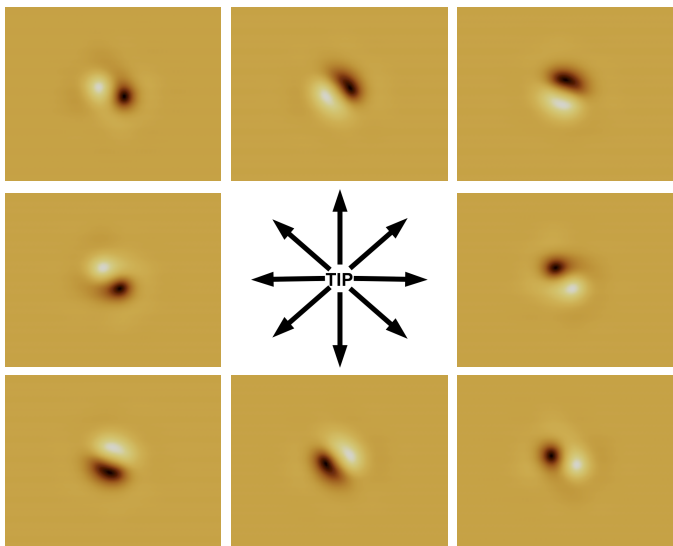


FIG. 5: (Color online) Same as Fig. 4 for the antiskyrmion with $Q = 1$.

Figures 4 and 5 show SP-STM images of the skyrmion in Fig. 1(a) with $Q = -1$ and of the antiskyrmion in Fig. 1(b) with $Q = 1$, respectively, by rotating the tip magnetization direction in the surface plane indicated by black arrows. We find that the two-lobes contrast is rotating in phase with the tip magnetization direction for the skyrmion and in anti-phase for the antiskyrmion, in agreement with Ref. [21]. The same finding holds when reversing the sign of P_{eff} (not shown) since in that case the individual image contrasts are inverted, and this does not affect the rotation direction of the STM contrasts upon in-plane tip magnetization rotation. This means

that the STM contrast rotation rule first identified by Dupé et al. [21] is insensitive to the sign of $P_{eff} = P_S P_T$ and, thus, to the sign of the surface and tip spin polarizations. This enables the straightforward determination of the sign of Q based on a series of SP-STM measurements performed with rotated in-plane sensitive magnetic tips: using our definition for the topological charge (Ref. [24]), an in-phase rotation of the contrast denotes $Q < 0$, i.e., skyrmion, and an anti-phase rotation of the contrast denotes $Q > 0$, i.e., antiskyrmion. Note that two in-plane tip magnetization orientations are already sufficient to provide this information, given that these orientations are linearly independent.

Figures 6, 7 and 8 show SP-STM images of the antiskyrmion in Fig. 1(c) with $Q = 2$, of the skyrmion in Fig. 1(d) with $Q = -2$, and of the skyrmion in Fig. 1(e) with $Q = -3$, respectively, by rotating the tip magnetization direction in the surface plane indicated by black arrows. We find the previously identified rule for the STM contrasts: in-phase rotation with the tip magnetization direction for the skyrmions ($Q < 0$) and anti-phase rotation for the antiskyrmion ($Q > 0$). Note that the number of bright and dark spots ($|Q|$ each) and their alternating order along the perimeter are preserved during the tip magnetization rotation, and this suggests that $|Q|$ can be determined from a single SP-STM measurement with a magnetic tip of any in-plane direction.

A special case is the “chimera” skyrmion in Fig. 1(f) with $Q = 0$. SP-STM images of this spin structure are shown in Figure 9 by rotating the tip magnetization direction in the surface plane indicated by black arrows. Here, we find that the skyrmionic (lower right) and antiskyrmionic (upper left) parts of the “chimera” skyrmion obey the rotation rules identified above, i.e., the skyrmionic part shows in-phase and the antiskyrmionic part shows anti-phase rotation of the contrast with respect to the rotation of the in-plane tip magnetization direction. This, however, results in a non-preserved number of bright and dark spots upon tip magnetization rotation. In most of the images there are either two bright and one dark spots, or the opposite composition: two dark and one bright. The existence of images with an equal number of bright and dark contrast regions, e.g., one-one bright and dark in the lower left and upper right images in Fig. 9, makes the identification of the “chimera” skyrmion difficult from a single SP-STM measurement as an image with such a contrast can also indicate a skyrmion with $Q = -1$ or an antiskyrmion with $Q = 1$. Another case is when the tip magnetization direction is in line with the axis of the “chimera” skyrmion (150 or -30 degrees with respect to the $+x$ [110] axis, see Fig. 3(d) of Ref. [24]), where two bright and two dark spots are observed (not shown). Such a magnetic contrast can also indicate a skyrmion with $Q = -2$ or an antiskyrmion with $Q = 2$. Nevertheless, as shown above, the in-plane rotation of the tip magnetization is quite helpful in the identification of the topological charge of real-space magnetic textures.

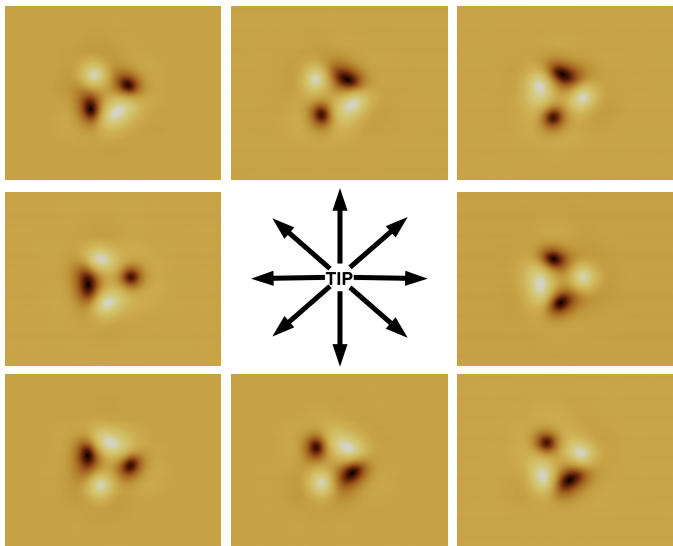


FIG. 6: (Color online) Same as Fig. 4 for the antiskyrmion with $Q = 2$.

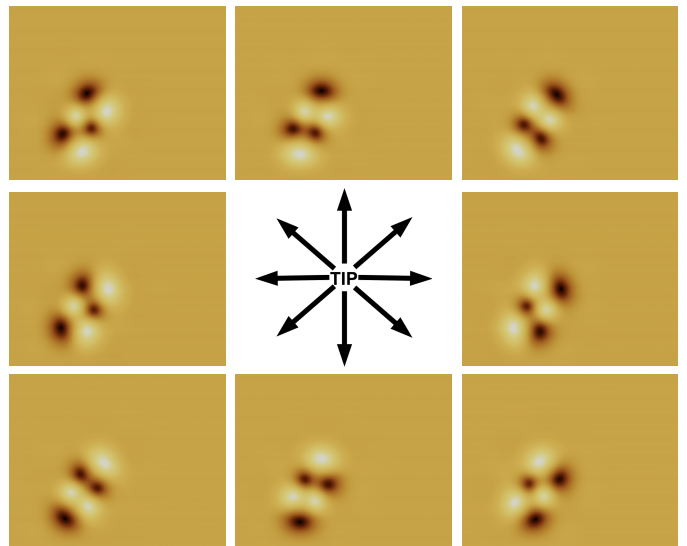


FIG. 8: (Color online) Same as Fig. 4 for the skyrmion with $Q = -3$.

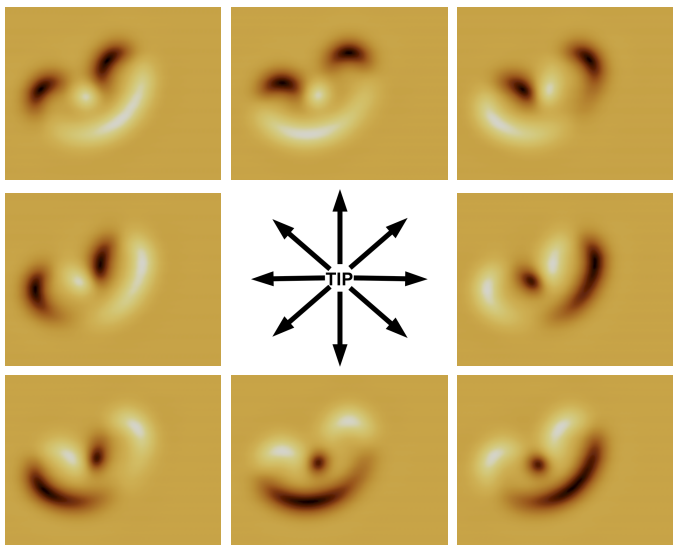


FIG. 7: (Color online) Same as Fig. 4 for the skyrmion with $Q = -2$.

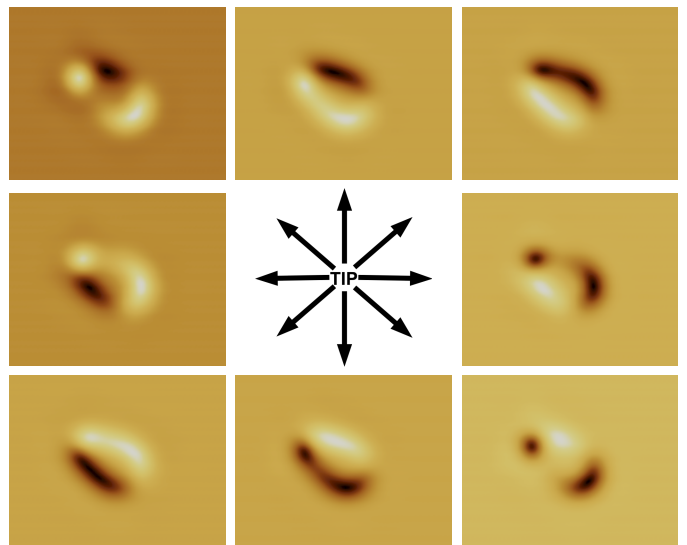


FIG. 9: (Color online) Same as Fig. 4 for the “chimera” skyrmion with $Q = 0$.

Based on our above findings, we suggest that if a single SP-STM measurement with an in-plane sensitive magnetic tip provides unequal numbers of bright and dark contrast regions then it can be excluded that the imaged spin structure has a $Q \neq 0$ topological charge. Additionally, the detection of a non-preserved number of bright and dark contrast regions upon in-plane tip rotation suggests a topological charge of $Q = 0$. These suggestions are, however, not generally true and apply to skyrmions formed in isotropic environment only. We have to stress that the shape of the magnetic skyrmions formed in anisotropic environments, e.g., in reconstructed films [23, 25], considerably affects the observed in-plane STM contrast and our above statements. Such an example is

an axially non-symmetric spin structure derived from experimental STM contrasts in Ref. [23], which shows both equal and unequal numbers of bright and dark contrast regions imaged with in-plane magnetized tips. A deeper theoretical analysis puts forward that the observed spin structure is indeed a magnetic skyrmion with $|Q| = 1$ exhibiting a non-circular shape [25]. It is interesting to note the similarity of the out-of-plane STM contrast of this reported skyrmion and our skyrmion with $Q = -2$ [see Fig. 2(d)]. The comparison of the in-plane contrasts in Fig. 7 and those of Ref. [23], however, excludes the $Q = -2$ skyrmion in the experiment. The reason for the distorted shape of the skyrmions in the experiment is the modified exchange interactions due to the reconstructed geometry

of the magnetic film. A similar effect has also been observed in another complex magnetic (spin spiral) state in a confined geometry [39]. We propose that theoretical calculations of such geometrically modified exchange interactions will explain the formation of distorted real-space magnetic textures in the future.

IV. CONCLUSIONS

We have investigated metastable skyrmionic spin structures with various topological charges ($Q = -3, -2, -1, 0, +1, +2$) in the $(\text{Pt}_{0.95}\text{Ir}_{0.05})\text{Fe}/\text{Pd}(111)$ ultrathin magnetic film by means of spin-polarized scanning tunneling microscopy (SP-STM) simulations. We found that an out-of-plane magnetized tip already results in distinguished STM contrasts for the different skyrmions. Using an in-plane magnetized tip, we have demonstrated that the magnitude of the topological charge can be determined from the image contrast of a single SP-STM measurement: the number of bright and dark contrast regions alternating along the perimeter of the skyrmion equals $|Q|$ each. We highlighted that an in-plane tip magnetization rotation provides the sign of Q independently on the sign of the effective spin polarization in the tunnel junction: in-phase rotation of

the contrast with respect to the tip magnetization indicates skyrmions ($Q < 0$) and anti-phase rotation antiskyrmions ($Q > 0$). A special case has been identified, the “chimera” skyrmion with $Q = 0$ exhibiting a skyrmionic and an antiskyrmionic part, where the number of bright and dark contrast regions is not preserved upon in-plane tip magnetization rotation. We propose that our STM contrast rules are general for skyrmionic structures in other ultrathin films providing an isotropic environment, and they are not valid in anisotropic environments of skyrmion formation, e.g., in reconstructed or confined film geometries. Our results for the identification of the topology of skyrmionic structures can prove to be useful for engineering skyrmions in ultrathin films for practical applications in the future.

V. ACKNOWLEDGMENTS

Financial support of the SASPRO Fellowship of the Slovak Academy of Sciences (project no. 1239/02/01), the Hungarian State Eötvös Fellowship of the Tempus Public Foundation (contract no. 2016-11) and the National Research, Development and Innovation Office of Hungary under Project Nos. K115575 and PD120917 is gratefully acknowledged.

-
- [1] S. Mühlbauer, B. Binz, F. Jonietz, C. Pfleiderer, A. Rosch, A. Neubauer, R. Georgii, P. Böni, *Science* 323, 915-919 (2009).
 - [2] W. Münzer, A. Neubauer, T. Adams, S. Mühlbauer, C. Franz, F. Jonietz, R. Georgii, P. Böni, B. Pedersen, M. Schmidt, A. Rosch, C. Pfleiderer, *Phys. Rev. B* 81, 041203 (2010).
 - [3] S. Seki, X.Z. Yu, S. Ishiwata, Y. Tokura, *Science* 336, 198-201 (2012).
 - [4] T. Adams, A. Chacon, M. Wagner, A. Bauer, G. Brandl, B. Pedersen, H. Berger, P. Lemmens, C. Pfleiderer, *Phys. Rev. Lett.* 108, 237204 (2012).
 - [5] X.Z. Yu, Y. Onose, N. Kanazawa, J.H. Park, J.H. Han, Y. Matsui, N. Nagaosa, Y. Tokura, *Nature* 465, 901-904 (2010).
 - [6] X.Z. Yu, N. Kanazawa, Y. Onose, K. Kimoto, W.Z. Zhang, S. Ishiwata, Y. Matsui, Y. Tokura, *Nature Mater.* 10, 106-109 (2011).
 - [7] S.X. Huang, C.L. Chien, *Phys. Rev. Lett.* 108, 267201 (2012).
 - [8] A. Fert, V. Cros, J. Sampaio, *Nature Nanotech.* 8, 152-156 (2013).
 - [9] N. Nagaosa, Y. Tokura, *Nature Nanotech.* 8, 899-911 (2013).
 - [10] X. Zhang, M. Ezawa, Y. Zhou, *Sci. Rep.* 5, 9400 (2015).
 - [11] L. Rózsa, E. Simon, K. Palotás, L. Udvardi, L. Szunyogh, *Phys. Rev. B* 93, 024417 (2016).
 - [12] S. Rohart, J. Miltat, A. Thiaville, *Phys. Rev. B* 93, 214412 (2016).
 - [13] C. Moreau-Luchaire, C. Moutafis, N. Reyren, J. Sampaio, C.A.F. Vaz, N. Van Horne, K. Bouzehouane, K. Garcia, C. Deranlot, P. Warnicke, P. Wohlhüter, J.-M. George, M. Weigand, J. Raabe, V. Cros, A. Fert, *Nature Nanotech.* 11, 444-448 (2016).
 - [14] S. Heinze, K. von Bergmann, M. Menzel, J. Brede, A. Kubetzka, R. Wiesendanger, G. Bihlmayer, S. Blügel, *Nature Phys.* 7, 713-718 (2011).
 - [15] S. Polesya, S. Mankovsky, S. Bornemann, D. Ködderitzsch, J. Minár, H. Ebert, *Phys. Rev. B* 89, 184414 (2014).
 - [16] B. Dupé, M. Hoffmann, C. Paillard, S. Heinze, *Nature Commun.* 5, 4030 (2014).
 - [17] E. Simon, K. Palotás, L. Rózsa, L. Udvardi, L. Szunyogh, *Phys. Rev. B* 90, 094410 (2014).
 - [18] S. Polesya, S. Mankovsky, D. Ködderitzsch, W. Bensch, H. Ebert, *Phys. Status Solidi RRL* 10, 218-221 (2016).
 - [19] K. von Bergmann, A. Kubetzka, O. Pietzsch, R. Wiesendanger, *J. Phys. Condens. Matter* 26, 394002 (2014).
 - [20] N. Romming, A. Kubetzka, C. Hanneken, K. von Bergmann, R. Wiesendanger, *Phys. Rev. Lett.* 114, 177203 (2015).
 - [21] B. Dupé, C.N. Kruse, T. Dornheim, S. Heinze, *New J. Phys.* 18, 055015 (2016).
 - [22] N. Romming, C. Hanneken, M. Menzel, J.E. Bickel, B. Wolter, K. von Bergmann, A. Kubetzka, R. Wiesendanger, *Science* 341, 636-639 (2013).
 - [23] P.-J. Hsu, A. Kubetzka, A. Finco, N. Romming, K. von Bergmann, R. Wiesendanger, arXiv:1601.02935 (2016).
 - [24] L. Rózsa, K. Palotás, A. Deák, E. Simon, R. Yanas, L. Udvardi, L. Szunyogh, U. Nowak, arXiv:1609.07012 (2016).
 - [25] J. Hagemeister, E.Y. Vedmedenko, R. Wiesendanger,

- arXiv:1603.01045 (2016).
- [26] K. Palotás, G. Mándi, W.A. Hofer, *Front. Phys.* 9, 711-747 (2014).
- [27] K. Palotás, W.A. Hofer, L. Szunyogh, *Phys. Rev. B* 84, 174428 (2011).
- [28] J. Tersoff, D.R. Hamann, *Phys. Rev. Lett.* 50, 1998-2001 (1983).
- [29] J. Tersoff, D.R. Hamann, *Phys. Rev. B* 31, 805-813 (1985).
- [30] S. Heinze, *Appl. Phys. A* 85, 407-414 (2006).
- [31] J. Bardeen, *Phys. Rev. Lett.* 6, 57-59 (1961).
- [32] K. Palotás, G. Mándi, L. Szunyogh, *Phys. Rev. B* 86, 235415 (2012).
- [33] W.A. Hofer, *Prog. Surf. Sci.* 71, 147-183 (2003).
- [34] K. Palotás, W.A. Hofer, *J. Phys. Condens. Matter* 17, 2705-2713 (2005).
- [35] K. Palotás, *Phys. Rev. B* 87, 024417 (2013).
- [36] K. Palotás, W.A. Hofer, L. Szunyogh, *Phys. Rev. B* 85, 205427 (2012).
- [37] L. Rózsa, A. Deák, E. Simon, R. Yanes, L. Udvardi, L. Szunyogh, U. Nowak, arXiv:1606.02464 (2016).
- [38] S. Meckler, N. Mikuszeit, A. Pressler, E.Y. Vedmedenko, O. Pietzsch, R. Wiesendanger, *Phys. Rev. Lett.* 103, 157201 (2009).
- [39] A. Palacio-Morales, A. Kubetzka, K. von Bergmann, R. Wiesendanger, *Nano Lett.* DOI: 10.1021/acs.nanolett.6b02528 (2016).